SINGLE-VIEW RECAPTURED IMAGE DETECTION BASED ON PHYSICS-BASED FEATURES

Xinting Gao, Tian-Tsong Ng, Bo Qiu

Institute for Infocomm Research
A*STAR, Singapore
Emails: {xgao, ttng, qiubo}@i2r.a-star.edu.sg

Shih-Fu Chang

Department of Electrical Engineering
Columbia University, USA
Email: sfchang@ee.columbia.edu

ABSTRACT

In daily life, we can see images of real-life objects on posters, television, or virtually any type of smooth physical surfaces. We seldom confuse these images with the objects per se mainly with the help of the contextual information from the surrounding environment and nearby objects. Without this contextual information, distinguishing an object from an image of the object becomes subtle; it is precisely an effect that a large immersive display aims at achieving. In this work, we study and address a problem that mirrors the above-mentioned recognition problem, i.e., distinguishing images of true natural scenes and those from recapturing. Being able to detect recaptured images, robot vision can be more intelligent and a single-image-based counter-measure for re-broadcast attack on a face authentication system becomes feasible. This work is timely as the face authentication system is getting common on consumer mobile devices such as smart phones and laptop computers. In this work, we present a physical model for image recapturing and the features derived from the model are used in a recaptured image detector. Our physics-based method out-performs a statistics-based method by a significant margin on images of VGA (640×480) and QVGA (320×240) resolutions which are common for mobile devices. In our study, we find that apart from the contextual information, the unique properties for the recaptured image rendering process are crucial for the recognition problem.

Keywords— Recaptured image detection, re-broadcast detection, image forensics, image recapturing model

1. INTRODUCTION

We rarely mistake the image of an object as the object itself in real life. For example, when we see an image of a car on poster pasted on a wall, we do not mistake it as a real car. Various types of contextual information including the size of the car image, the fact that the car image is on the wall, the flatness of the image that appears to our stereo vision, and the way light is reflected from the poster surface helps us in making this judgement. However, if we strip away the contextual information as much as possible as in a large immersive display setting, we may confuse the flat image of the car as the car per se, despite our stereo vision. With minimum contextual information, recognizing the two through mono-vision, e.g., viewing through a camera, would be much more challenging. In

(a) The pipeline to produce a real-scene image.

(b) The pipeline to produce a recaptured image.

Fig. 1. The generative process for the two classes of images used in our work.

this paper, we study the problem of distinguishing two image classes, i.e., images of true natural scenes and the recaptured natural-scene images on a computer. The process of generating the two classes of images is shown in Fig. 1. Most people consider this recognition task as difficult or even impossible with single-view vision. Indeed, in computer vision, extracting 3-dimensional (3D) geometry from a single image is ill-posed. Without explicitly extracting (reconstructing) the 3D geometry, our new method utilizes the contextual information and the rendering process related properties to distinguish the two image classes based on a single-view image. Single-view recaptured image detection or recognition is an enabling technology for a few important applications. First, it provides additional information for a robot or an unmanned vehicle to distinguish an image of an object from the object per se. Second, the current research for general object-class recognition [1] does not consider recaptured image as a separate image class, and hence a poster cannot be in general detected. In this case, single-view recaptured image detection can be applied as a pre-filter for an object recognizer. Third, presenting a printed face to a face authentication system as an attempt to gain illegal access into the system is a well-known attack and single-view recaptured image detection can be applied as a counter-measure to this form of attack. Face authentication system has recently been adopted for access control on mobile devices such as laptop computers and smart phones. Such authentication system is designed for fast response time and often not equipped with sophisticated liveness detection for verifying a live face. Recently, a Vietnamese

security group found that most commercial laptop computers with face authentication system can be easily attacked by just presenting a human face printed on an A4-size paper [2].

In this work, we propose a physics-based approach for single-view recaptured image detection which exploits the contextual information remaining on a recaptured image and the unique properties of the recaptured image rendering process. The set of physics-based features is composed of the contextual background information, the spatial distribution of specularity that is related to the surface geometry, the image gradient that captures the non-linearity in the recaptured image rendering process, the color information and contrast that is related to quality of reproduction rendering, and a blurriness measure that is related to the recapturing process. The physics-based method outperforms the statistical method proposed in [3] by more than 10% when minimum contextual information is used. We also perform a detailed analysis of each individual physics-based feature.

Our work is presented as follows. We will review the prior work in Sec. 2. In Sec. 3, a physical model for the recapturing process and the related physics-based features are described in detail. Sec. 4 describes the dataset that we collected for evaluating our method and shows the experiments which compare our method with a statistics-based method. In Sec. 5, the limitations of the current dataset and method are discussed and future works are described. Finally, we give conclusions in Sec. 6.

2. PRIOR WORK

Our work is related to the prior work in single-view recaptured image detection, liveness detection for face authentication, and device identification in digital image forensics.

2.1. Single-view Recaptured Image Detection

In [3], Farid and Lyu performed an experiment on classifying photographic images and scanned images using wavelet statistical features which capture the deviation from the normal image statistics resulted from the image scanning process. The method could classify the two image classes with an average accuracy of 99.6%. This method is statistical in nature therefore it does not admit to physical intuitions that can lead to further ideas on improving the method. In [4], Ng et al. devised a set of physics-motivated features to classify photographic images and photorealistic computer graphic images. They showed that the physics-motivated features has the capability of distinguishing computer graphics recaptured from an LCD display when the recaptured images have a resolution high enough to resolve the grid structure of the display. In [5], Yu et al. proposed a way to extract the micro-texture on the A4-size printing paper from the specularity component of a recaptured image. Later in [6], Bai et al. assessed the method on a dataset consisting of 65 human face images where the method showed 2.2% False Acceptance Rate and 13% False Rejection Rate of the recaptured images. The method proposed by Yu et al. requires the input images to

have a high enough resolution in order to resolve the fine micro-texture of printing papers and its performance may be unreliable on images other than face images with limited amount of fine texture.

In contrast to the statistical deviation and the appearance of fine textures on the display medium, the physics-based features that we propose in this work exploit the contextual information and the characteristics of the image recapturing process for recognizing recaptured images. This method works well on low-resolution images of natural scenes.

2.2. Liveness Detection for Face Authentication Systems

Re-broadcast attack where an attacker presents a printed face in an attempt to intrude a face authentication system is well-known and well-studied. The existing counter-measures mainly rely on ways to assess the level of liveness of the presented face. These methods require a sequence of image frames for liveness detection. For example, in [7], eye blinks are used to identify the liveness of a subject. Although these methods are effective in detecting a static face re-broadcast attack, they are vulnerable to video replay attack. The single-view recaptured image detection method in this work requires only a single input image and therefore is effective against video replay attack.

2.3. Device Identification

Image recapturing process consists of image printing or displaying followed by re-photographing. We can consider this process as a means of color image rendering, just like computer graphic rendering or half-toning. In the area of digital image forensics, the class of methods that analyze an image to recognize how the image is generated is classified as image source or device identification. These methods attempt to identify the camera characteristics inherent in an image [8], the printer/scanner signatures [9] or characteristics of computer graphics rendering [4]. In this work, we consider recaptured images produced by a camera under uncontrolled lighting and paper positioning, in contrast to the controlled setting for image scanning.

3. A PHYSICAL MODEL FOR IMAGE RECAPTURING PROCESS

A cascaded dichromatic model [5] was proposed to explain the origin of the micro-texture on a paper surface which appears mainly in the specularity component of a recaptured image. However, to resolve the micro-texture, the recaptured image needs to have a sufficiently high resolution. Such high-frequency characteristic of a display medium is merely one of the many physical properties of a recaptured image. To explain these properties in a comprehensive manner, a more general physical model is needed for the image recapturing process.

3.1. A General Image Recapturing Model

As shown in Fig. 1 (b), a recapturing process involves three stages, i.e., the first capture, the display, and the second cap-

ture or recapture. Assume that the first capture is performed using any camera c_1 of any resolution and type, the display is done through a medium m and the second capture is performed using a camera c_2. The scene radiance of the first capture, J_1, is captured by c_1 to produce a digital image

$$I_1(x) = f_1(J_1(x)), \quad (1)$$

where f_1 is the camera response function for c_1. I_1 is reproduced on a medium m and the reproduced image is not exactly the same as I_1 due to the limitation of the reproduction devices such as printers and LCD display. The reproduced image on m can be written as

$$I_m(x) = f_m(I_1(x)). \quad (2)$$

Note that the surface property of the reproduced image on medium m can be drastically different from that of the original 3D scene that gives rise to J_1. When I_m is displayed in the real-world and illuminated by the environment light, the way the incident light is reflected from the display medium m is determined by the surface property of m and the reflected radiance may be different from I_m. For instance, the specular fine texture that is observed on a recaptured image is due to both the spatial and reflectance properties of the printing paper. Considering such deviation from I_m, we can model the reflected radiance observed by the second camera c_2 as

$$I_{recap}(x) = f_2(I_m(x)\alpha(x) + R(x)(1 - \alpha(x))), \quad (3)$$

where f_2 is the camera response function of c_2, R is the radiance arising from the recapturing setting and the display medium, and α weights the effect of R. R accounts for the specular fine texture of a printing paper, the backlight that transmits through the paper, as well as the large region of highlights arises from the flat geometry of the printing paper. Furthermore, when the real scene around the reproduced image I_m is captured by c_2, the region other than I_m can also be modelled by R.

3.2. Features Inspired by the General Model

As shown in Fig. 1 (a), for producing a real-scene image, we simply capture the scene radiance, J_1, using the end-user camera c_2,

$$I_{real}(x) = f_2(J_1(x)). \quad (4)$$

While the complete recaptured model can be obtained from Eq. (3) by replacing I_m with Eq. (1) and I_1 with Eq. (2),

$$I_{recap}(x) = f_2(f_m(f_1(J_1(x)))\alpha(x) + R(x)(1 - \alpha(x))). \quad (5)$$

Contrasting Eq. (4) and Eq. (5) gives us clues for detecting the recaptured image from the real-scene image. The clues include the difference in the radiometric non-linearity arising from the various response functions f_1, f_2 and f_m, the possible backlight and patches of highlight for a recaptured image, the contextual information from the background scene of a recaptured image, the distinct properties of the display medium for a recaptured image, chromatic properties of the printing devices, and so on. The following section describes features that characterize the above-mentioned properties.

3.3. Physics-based Features

From the application point of view, a single-view recaptured image detector may be used in uncontrolled lighting and varying background environment. For example, the laptop user may perform face authentication anytime and anywhere. If the attacker uses an LCD screen to display the first capture, the brightness of the screen can be adjusted to achieve the best effect. Furthermore, the attacker may use any method and device to get the first capture. Therefore, the features for recaptured image detection should be general and not restricted to a specific setting. Specifically, the features for describing the photometric properties of a recaptured image should cater for diverse lighting conditions, and the device-related features should be capable of modeling various devices. Since a recaptured image could be of any natural scene, the features should be image-content independent. Bearing in mind these desired properties, we do not make specific assumption on lighting, types of printing or imaging devices, and image content when devising the following set of features.

3.3.1. Background Contextual Information

Some portion of a recaptured image may contain the real scene background, which can be considered as a form of contextual information. The background portion is generally different from the display medium with reproduced content. By assuming that the display medium is usually at the center, the background contextual information and its contrast to the display medium portion can be exploited by dividing an input image into $M \times N$ non-overlapping blocks and extract features from each of the blocks independently. The contrast between the bordering background portion and the central display medium portion will reflect on the spatial distribution of the features.

3.3.2. Spatial Distribution of Specularity

It has been shown that specularity distribution on a surface is indicative of its geometry [10]. As the geometry of a display medium is commonly flat, the specularity distribution for a recaptured image could be different from that of a real-scene image as the real-scene objects may not be flat. Another cause of difference for specularity distribution is due to the image recapturing process. In general, the specularity observed in a recaptured image is a superposition of the specularity from the first capture and that from the second capture (recapture). The superposition of specularity may result in a distinctive spatial distribution. Fig. 2 shows an example of such effect. Fig. 2 (a) and (b) are respectively a real-scene image and its corresponding recaptured image. Fig. 2 (c) and (d) are the specular component (contrast-adjusted for clearer visualization) extracted respectively from images in Fig. 2 (a) and (b) using Tan et al's method of diffuse-specular decomposition [11]. The food in the bowl shows little specularity in the real-scene image. During the image recapturing process, secondary specularity gives rise by the direct reflection from the printing paper is homogeneously distributed across the recaptured image. As a result, specularity
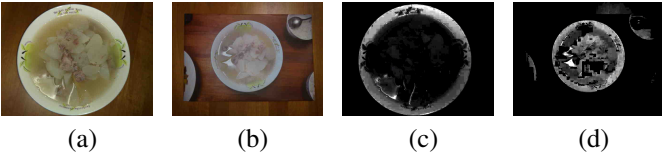
Fig. 2. An example to explain the spatial distribution of specularity. (a) Real-scene image. (b) Recaptured image. (c) Specular component of the image shown in (a). (d) Specular component of the image shown in (b). The spatial distribution is more homogeneous in (d) than in (c).

is seen across the bowl portion. To extract this feature, we first decompose the image using Tan et al.'s method to get the specular component, I_s [11]. As regions with homogenous intensity such as the bright blue sky for an outdoor scene and the portion of the image suffering from saturation are often mistakenly extracted as specularity, we only consider the specularity in the regions with higher gradient measure and within the intermediate intensity range, $1.5 * \mu_{I_s} < I_s < 4 * \mu_{I_s}$, where μ_{I_s} is the mean of the specularity image. The ratio of specularity in an image block is computed as a feature with dimension one.

3.3.3. Surface gradient

If we consider image recapturing as an image rendering process, it would have a different non-linear response compared to that of a camera. From Eq. (5), we can see that the non-linear response of a recaptured image is a composite of the responses from the first camera, the intermediate printing, and the second camera, while the the non-linear response of a real-scene image only comes from second camera, i.e., the end-user camera. In [4], Ng et al. showed that the non-linearity on the response can be characterized using the image gradient or more effectively using the image gradient on the image manifold. Therefore, we include image gradient in our physics-based feature set. The dimension of the surface gradient feature is 31. Due to the high dimensionality, we extract the feature from the image globally instead of from each individual block.

3.3.4. Color histogram

As we know, the color gamut is different for different color rendering devices [12]. During the stage of reproducing the image content on a physical medium, both f_1 and f_m may introduce some device related color signatures. Fig. 3 shows two examples of how f_m may introduce some color features into the recaptured image. Fig. 3 (a) shows a real-scene image, while Fig. 3 (b) and (c) show the corresponding recaptured images where the first-capture image is respectively printed on an office printing paper using a laser color printer and displayed on an LCD display. It is observed that the color printer introduces some red tint into the recaptured image, while the LCD screen introduces some blue tint into the recaptured image. To extract this feature, the $3 \times 3 \times 3$ HSV color histogram of an image

is computed on each image block. The dimension of this color feature within each block is 9.
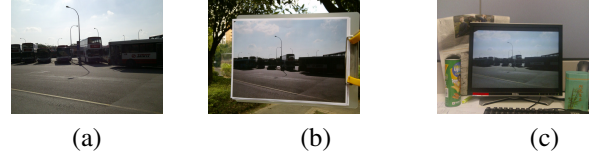
Fig. 3. Examples to explain the color features introduced by the content reproduction process. (a) Real-scene image. (b) Recaptured image in which the attack picture is printed on an office printing paper using a laser color printer. (c) Recaptured image in which the attack picture is displayed on an LCD screen. The printer introduced the red tint in (b) while the LCD display introduced the blue tint in (c).

3.3.5. Contrast

A recent study shows that the laser printer has a lower contrast ratio than an actual real scene [12], and this represents another feature of the content reproduction devices. To extract the contrast in each block, the image is first transformed into a gray level image. Within each block of the image, local contrast, i.e., the ratio of the maximum to the minimum value, is computed in the $n \times m$ non-overlapping sub-blocks. The maximum local contrast within each block is taken as the contrast measurement of the block. The dimension of contrast feature within each block is 1.

3.3.6. Chromaticity

As pointed out in [12], the color gamut for the real scene and various types of color reproduction devices are significantly different. They correspond to different color coverage on the CIE 1931 x-y chromaticity space which is shown in Fig. 4. The white point $(x,y) = (\frac{1}{3}, \frac{1}{3})$ in the chromaticity space corresponds to a color with equal energy for the three primary colors, while the boundary of the horse-shoe-shaped color space corresponds to fully saturated colors. We model the extent and shape of the color coverage for an image with the covariance of the image color distribution in the CIE 1931 x-y chromaticity space by assuming the center being the white point. To extract the chromaticity covariance features, an RGB image is first transformed into the CIE XYZ color space and the chromaticity components, $x = \frac{X}{X+Y+Z}$ and $y = \frac{Y}{X+Y+Z}$ are calculated. We then compute the covariance of the (x,y) color by assuming the white point as the center. A 2×2 symmetric covariance matrix is computed from every block and the three unique elements in the upper triangular portion of the covariance matrix are used as the chromaticity feature.

3.3.7. Blurriness

There are three possible scenarios that blurriness can arise in a recaptured image. First, the first capture device or the printing
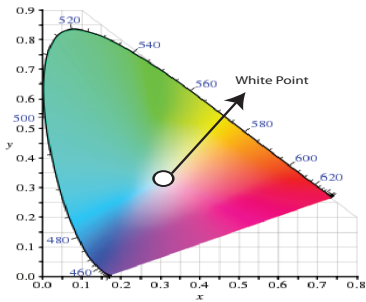
Fig. 4. CIE 1931 x-y chromaticity space (original image courtesy of Wikipedia).

device could be of low resolution. Second, the attack image may be small and the display medium may have to be placed outside of the focus range due to a specific recaptured setting. For example, if the intruder uses the small-size photo on a badge or IC (Identity Card) to intrude a face authentication system, the photo must be placed close to the end-user camera to imitate a life-size human face. In this setting, the display medium may not be in the focus range of the camera. Third, if the end-user camera has a limited depth of field, the distant background may be blur, while the entire display medium is in focus. In this case, the in-focus region is more likely to be of a regular shape, e.g., a rectangular focus region for a printing paper, in contrast to a less regular shape of a 3D object, e.g., silhouette of a human face. The spatial distribution of a blur measure proposed by Crete et al. [13] extracted from each image block will form a clue for detecting the above-mentioned scenarios. The dimension of blur feature within each block is 1.

4. DATASET AND EXPERIMENTS

4.1. Natural-Scene Recaptured Image Dataset

We constructed a recaptured image dataset of natural scene in which human face images form a subset. The dataset includes outdoor natural scene, indoor office or residence scene, and close-up or distant scene. The dataset was produced with 3 camera phones (Acer M900, Nokia N95, and HP iPAQ hw6960) which are set to auto mode whenever possible. The general resolution of the dataset images is set to VGA (640×480). The Acer M900 and Nokia N95 phone have a back-facing camera and a low-resolution front-facing camera, while HP iPAQ hw6960 has only a back-facing camera. Therefore, the three camera phones give us five distinct cameras. The resolution of the Nokia N95 front-facing camera is of a QVGA (320×240) resolution. The quality of the images depends on both the sensor resolution and the lens quality. For example, the QVGA-resolution images of the Nokia N95 front-facing camera appear to be of a better quality than the VGA-resolution images of the Acer M900 front-facing camera. For some of the recaptured images, we try to match the background with the content on the printed image, with the intention of minimizing the effect of the background contextual contrast. In our recapturing setup, we

use a Nikon D90 single-lens reflex (SLR) camera to produce images of 3216×2136 resolution as the first capture and HP CP3505dn laser color printer of 1200×600 dpi for printing of office paper. The high-quality first-capture camera and printer ensure high-quality image on the printing paper with minimum artifacts. For recapturing, we use the above mentioned camera phones as the end-user device. The dataset is balanced in the sense that we have the same image content in the real-scene and recaptured image sets, with the intention for minimizing the inter-class content discrepancy.
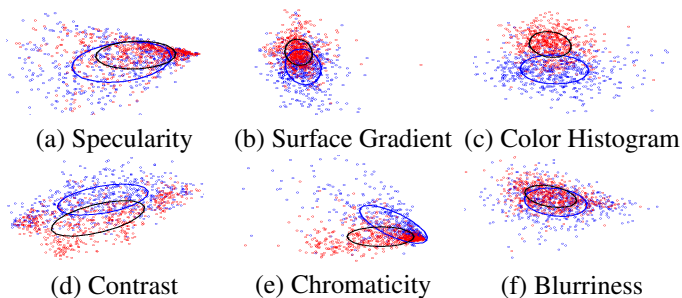
4.2. Experiments

We group the five distinct phone cameras into the categories of front-facing cameras and back-facing cameras. We get 608 real-scene images and 589 recaptured images for back-facing cameras, and 420 real-scene images and 410 recaptured images for front-facing cameras. We compare the performance of our features and the wavelet statistical features [3] through SVM classifications of the two image classes, i.e., real-scene and recaptured. A 3×3 block structure is used for modeling the background contextual information when extracting the physics-based features. The dimension of the proposed physics-based features and the wavelets statistical features are respectively 166 and 216. The results shown in Table 1 (a) are the average accuracy for ten independent iterations of SVM classification with random data partition and five-fold cross-validation. For both front and back-facing cameras, the physics-based features outperform the wavelet statistical features with a significant margin. To further analyze the effectiveness of the scheme

Table 1. Results of dataset captured by smart phone cameras.

Smart phone cameras	front	back
(a) Original dataset		
Proposed physical features (166dim)	**91.3%**	**95.0%**
Wavelets statistical features (216dim)	84.6%	88.0%
(b) Dataset: images are cropped at the central quarter		
Proposed physical features (166dim)	**76.2%**	**80.2%**
Wavelets statistical features (216dim)	67.6%	71.1%
(c) Dataset: images are cropped at the top-left quarter		
Proposed physical features (166dim)	**86.8%**	**93.5%**
Wavelets statistical features (216dim)	70.8%	81.6%

and features of the proposed method, we linearly project each type of the features to a 2D space through Fisher discriminant analysis. Fig. 5 shows the distribution of the six types of features described in Sec. 3.3. The ellipses in the figure depict the mean and the covariance of a single-class feature distribution. It is observed that color histogram and contrast are the most effective features for our dataset, while specularity and blurriness are less effective. To assess the capability of the methods without the background contextual information and the distinctive white border on the recaptured image, we extract the central portion of the image which are supposed to cover only the display medium

(a) Specularity   (b) Surface Gradient   (c) Color Histogram

(d) Contrast   (e) Chromaticity   (f) Blurriness

Fig. 5. 2D projection of the physical feature distribution for the real-scene image sets (red) and the recaptured image sets (blue).

in a classification experiment. As a comparison, we perform a similar experiment with the top-left portion of the image which has the same size as the central image. In contrast to the central portion, the top-left portion retains the background contextual information and the white border. The results are also shown in Table 1 (b) and (c). It is found that the background contextual information does contribute significantly when it comes to separating the two image classes.

5. DISCUSSIONS AND FUTURE WORKS

One limitation of our current dataset is that the scale of the recaptured images is smaller than the corresponding real images, e.g. images shown in Fig. 2 and Fig. 3. Another characteristics of the dataset is the white border in the attack image which is purposefully preserved in order to mimic a practical attack situation. The effect for the white border can be discounted if we extract only the central part of the recaptured image, as we did in Sec. 4.2. Our dataset collection effort is ongoing. We will introduce more diversity into the new dataset particularly in terms of the recapturing procedure by introducing more types of display medium and printing devices as well as different ways of positioning and capturing the display medium. Such diversity will diminish the effect of the above-mentioned biases.

We believe that our method has a great room for improvement and it can be easily extended by following the physical intuition of our method. For example, we have not exploited the photometric features such as specularity spatial distribution and surface gradient to the greatest extent. We will explore more sophisticated way of extracting the photometric features.

6. CONCLUSIONS

In this paper, we propose a general physical model for the image recapturing process, which provides a physical insight into the recaptured image detection. The features inspired by the general model achieve significantly better classification performance on the low resolution (VGA or QVGA) images as compared to the wavelet statistical features. We also present a dataset of recaptured and real-scene images obtained by camera phones as the end-user device. This dataset is suitable for evaluating methods

for recaptured image detection on mobile devices.

8. REFERENCES

[1] L. Fei-Fei, R. Fergus, and P. Perona, "One-shot learning of object categories," *IEEE Transactions on Pattern Analysis and Machine Intelligence*, vol. 28, no. 4, pp. 594–611, 2006.

[2] D. Ngo, "Vietnamese security firm: Your face is easy to fake," *http://news.cnet.com/8301-17938_ 105-10110987.html*, 2008.

[3] H. Farid and S. Lyu, "Higher-order wavelet statistics and their application to digital forensics," *IEEE Workshop on Statistical Analysis in Computer Vision*, 2003.

[4] T.-T. Ng, S.-F. Changand Y.-F. Hsu, L. Xie, and M.-P. Tsui, "Physics-motivated features for distinguishing photographic images and computer graphics," *ACM Multimedia*, 2005.

[5] H. Yu, T.-T. Ng, and Q. Sun, "Recaptured photo detection using specularity distribution," *IEEE International Conference on Image Processing (ICIP)*, 2008.

[6] J. Bai, T.-T. Ng, X. Gao, and Y.-Q. Shi, "Is physics-based liveness detection truly possible with a single image?," *IEEE International Symposium on Circuits and Systems (ISCAS)*, 2010.

[7] G. Pan, L. Sun, Z. Wu, and S. Lao, "Eyeblink-based anti-spoofing in face recognition from a generic webcamera," *IEEE International Conference on Computer Vision (ICCV)*, Oct. 2007.

[8] T.-T. Ng, "Camera response function signature for digital forensics Part II: Signature extraction," *IEEE Workshop on Information Forensics and Security (WIFS)*, 2009.

[9] N. Khanna and E. J. Delp, "Source scanner identification scanned documents," *IEEE Workshop on Information Forensics and Security (WIFS)*, 2009.

[10] M. Osadchy, D. Jacobs, R. Ramamoorthi, and D. Tucker, "Using specularities in comparing 3d models and 2d images," *Computer Vision and Image Understanding*, vol. 111, no. 3, pp. 275–294, 2008.

[11] R. Tan and K. Ikeuchi, "Separating reflection components of textured surfaces using a single image," *IEEE Transactions on Pattern Analysis and Machine Intelligence*, vol. 27, no. 2, pp. 178–193, 2005.

[12] O. Bimber and D. Iwai, "Superimposing dynamic range," *ACM Siggraph Asia*, vol. 27, no. 5, 2008.

[13] F. Crete, T. dolmiere, P. Ladret, and M. Nicolas, "The blur effect: perccption and estimation with a new no-reference percptual blur metric," *SPIE International Society for Optical Engineering*, 2007.